Keratan Sulfate Phenotype in the β-1,3-*N*-Acetylglucosaminyltransferase-7–Null Mouse Cornea

Stacy L. Littlechild,[1,2] Robert D. Young,[1,2] Bruce Caterson,[2,3] Hideyuki Yoshida,[4] Maya Yamazaki,[5] Kenji Sakimura,[5] Andrew J. Quantock,[1,2] and Tomoya O. Akama[4,6]

[1]Structural Biophysics Group, School of Optometry and Vision Sciences, College of Biomedical and Life Sciences, Cardiff University, Cardiff, Wales, United Kingdom
[2]Cardiff Institute of Tissue Engineering and Repair, Cardiff University, Cardiff, Wales, United Kingdom
[3]Connective Tissue Biology Laboratory, School of Biosciences, College of Biomedical and Life Sciences, Cardiff University, Cardiff, Wales, United Kingdom
[4]Department of Pharmacology, Kansai Medical University, Osaka, Japan
[5]Department of Cellular Neurobiology, Brain Research Institute, Niigata University, Niigata, Japan
[6]Tumor Microenvironment Program, Sanford Burnham Prebys Medical Discovery Institute, La Jolla, California, United States

Correspondence: Tomoya O. Akama, Department of Pharmacology, Kansai Medical University, Osaka 573-1010, Japan;
akamat@hirakata.kmu.ac.jp.

Submitted: July 28, 2017
Accepted: December 27, 2017

Citation: Littlechild SL, Young RD, Caterson B, et al. Keratan sulfate phenotype in the β-1,3-*N*-acetylglucosaminyltransferase-7–null mouse cornea. *Invest Ophthalmol Vis Sci*. 2018;59:1641–1651. https://doi.org/10.1167/iovs.17-22716

Purpose. Synthesis of keratan sulfate (KS) relies on coordinated action of multiple enzymes, including the *N*-acetylglucosamine–transferring enzyme, β-1,3-*N*-acetylglucosaminyltransferase-7 (β3GnT7). A mouse model deficient in β3GnT7 was developed to explore structural changes in KS and the extracellular matrix (ECM; i.e., the corneal stroma), elucidate the KS biosynthesis mechanism, and understand its role in corneal organization.

Methods. A knockout vector for the β3GnT7-encoding gene, *B3gnt7,* was created to develop heterozygous- (htz) and homozygous-null (null) knockouts. Epithelial, stromal, and whole cornea thicknesses were measured from each group. Proteoglycans were stained with cupromeronic blue for visualization by electron microscopy, and Western blot analyses were conducted on the KS core protein, lumican. Corneal sections were labelled fluorescently for KS and chondroitin sulfate/dermatan sulfate (CS/DS) using monoclonal antibodies 1B4 or 2B6, respectively.

Results. Wild-type (WT) and htz corneas were of similar stromal thickness, whereas null specimens measured relatively thin. Electron micrographs revealed that WT and htz samples contained comparable levels of KS- and CS/DS-PGs. Null corneas, however, lacked detectable KS and featured uncharacteristically elongated electron dense PG filaments, which were susceptible to chondroitinase ABC digestion. Western blotting revealed lumican in the null corneas was substituted with low-molecular-weight KS, relative to WT or htz tissue. KS was not immunohistochemically detectable in the null cornea, whereas CS/DS content appeared increased.

Conclusions. Addition of *N*-acetylglucosamine via β3GnT7 to KS glycosaminoglycans is necessary for their biosynthesis. Without β3GnT7, murine corneal stromas lack KS and appear to compensate for this loss with upregulation of chondroitinase ABC-sensitive PGs.

Keywords: chondroitin sulfate, extracellular matrix, glycosyltransferase, keratan sulfate, sulfotransferase

Keratan sulfate (KS) is an extracellular matrix (ECM) glycosaminoglycan (GAG) present in a host of tissues in many organisms spanning the animal kingdom. Its exact structure varies depending on the organism and tissue in which it is found (see Funderburgh 2002[1] for comprehensive review). The highest abundance of KS in the body is found in the cornea, where KS-GAGs covalently associate to core proteins lumican, keratocan, or mimecan via an *N*-linkage to asparagine (Asn) residues, thus forming a proteoglycan (PG). KS-GAGs are also commonly found in cartilage and brain, where their association to core proteins occurs via an *O*-linkage to serine (Ser) or threonine (Thr) residues.

The linkage region of corneal KS-GAGs is comprised of two *N*-acetylglucosamine (GlcNAc) residues, the innermost of which is fucosylated at its sixth carbon (C6).[1,2] Three mannose residues divide the molecule into its bi-antennary structure, from which its short and long arms extend (shown in Fig. 1). Both short and long arms contain GlcNAc and galactose residues linked in –3Galβ1,4GlcNAcβ1– conformation, also known as poly-*N*-acetyllactosamine.[3] The long arm of KS contains three regions of repeating disaccharides, distinguished by their degree of sulfation. The unsulfated region does not contain sulfate modification on GlcNAc or galactose and is one to two disaccharides long. The monosulfated region, however, is 10 to 12 disaccharides in length and carries sulfate groups at the C6 of GlcNAc residues. Sulfate moieties bind GlcNAc and, less frequently, galactose within the disulfated region of corneal KS-GAGs. The disulfated region varies in length and often terminates with a sialic acid capping structure.[2,4] The short arm of KS-GAGs lacks the mono- and disulfated regions described

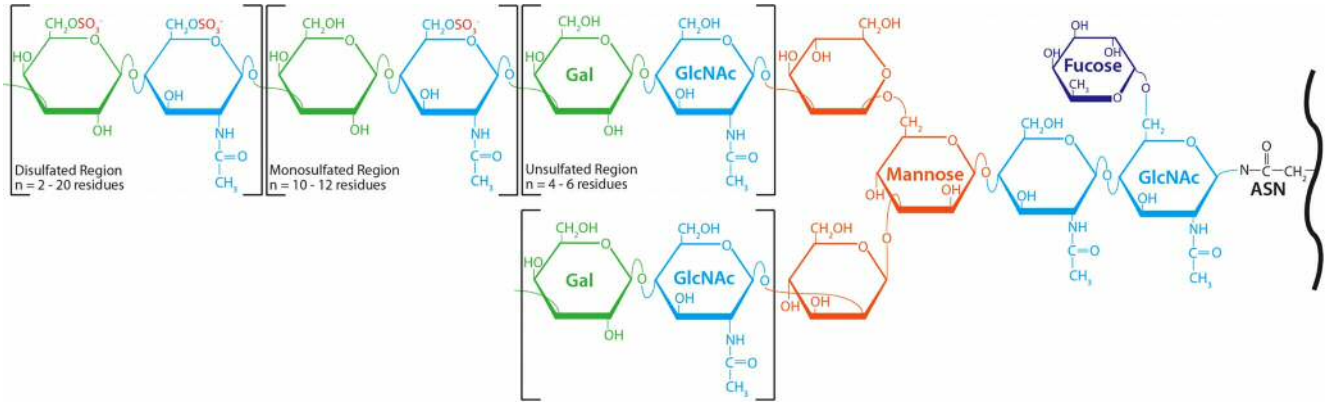

Figure 1. Structure of corneal KS-GAGs. Asparagine residues (ASN) within KS-PG core proteins (*black*) are bound via an *N*-linkage to two GlcNAc residues (*light blue*), followed by three mannose residues (*orange*), which divide the molecule into two arms. The innermost linkage GlcNAc is fucosylated at C6. The elongated (*top*) and short (*bottom*) arms both contain repeating GlcNAc and galactose (*green*) residues linked in –3Galβ1,4GlcNAcβ1– repeating fashion. Whereas these inner disaccharide repeats do not carry sulfate modification, GlcNAc residues in the monosulfated region of the molecule are sulfated at C6. The C6 positions of GlcNAc and most, but not all, galactose residues are modified by sulfate in the disulfated region of KS-GAGs.

above and instead terminates with sialic acid following one to two unsulfated disaccharide repeats.[5] The frequent substitution of sulfate groups along their carbohydrate backbones confers upon KS-GAGs their dense negative charge, and, in turn, their hydrophilicity.

Importantly, the sulfation status of KS can impact on tissue function; a prime example is where a disturbed KS sulfation pathway leads to progressive loss of vision as in the inherited disease macular corneal dystrophy.[6–10] The causative gene is *CHST6*, which encodes corneal GlcNAc 6-*O*-sulfotransferase (CGn6ST).[11,12] Consequences of the abnormally sulfated PG population include altered collagen architecture within the cornea and stromal opacifications, which can only be treated by a corneal graft. Structural matrix changes mimicking those seen in human corneas with macular corneal dystrophy have also been documented in mouse corneas lacking *Chst5,* which is the murine orthologue of the human CGn6ST-encoding gene.[13–15]

The apparent importance for properly formed KS has sparked recent interest in elucidating the biosynthetic mechanism that elongates and sulfates KS-GAGs. It is thought that at least four enzymes, including two glycosyltransferases and two sulfotransferases, are required for KS biosynthesis. A number of studies have posited that highly sulfated KS-GAGs are formed by addition of GlcNAc via β-1,3-*N*-acetylglucosaminyltransferase 7 (β3GnT7, encoded by *B3gnt7*) to the nonreducing terminus of the growing KS chain.[16] It is thought that CGn6ST (described above) subsequently sulfates the 6-*O* position of GlcNAc prior to galactose addition by β-1,4-galactosyltransferase 4 (β4GalT4, encoded by *B4galt4*). It is hypothesized that these three steps repeat, forming a chain of disaccharides singly sulfated on GlcNAc residues.[17,18] It has been suggested that galactose sulfation is achieved in a separate step, since the discovery that KS galactose 6-*O*-sulfotransferase (KSGal6ST, encoded by *Chst1*) preferentially sulfates internal, rather than terminal, galactose residues.[19,20]

The work herein furthers our understanding of corneal KS biosynthesis, specifically investigating the role of the glycosyltransferase β-1,3-*N*-acetyltransferase 7 (β3GnT7). Whereas previous work has demonstrated the GlcNAc-transferring capability of β3GnT7 in vitro, we generated a *B3gnt7*-null mouse and explored the consequences of this mutation in the cornea. Our results suggest that without the ability to elongate KS chains via addition of GlcNAc residues at their non-reducing termini, the normal corneal stromal KS-PG phenotype is abolished.

Methods

Knockout Mouse Production

Knockout vector for *B3gnt7* was prepared by recombineering technique.[21] Bacterial artificial chromosome (BAC) clones (RP24-231G17 and RP24_144F16), which included *B3gnt7*, were obtained from BACPAC resources (Children's Hospital Oakland Research Institute, Oakland, CA, USA). Because most of the protein coding sequence is encoded on exon 2 of the gene, the loxP sequence was inserted before and after exon 2. A neo cassette, which consists of flippase recombinase target (FRT)-phosphoglycerate kinase promoter (PGK)-neomycin resistant gene (neo)-FRT was also inserted downstream of exon 2. The DNA fragment containing modified *B3gnt7* was retrieved to pBSII-DTA vector and used as a knockout vector. This vector was introduced into RENKA mouse embryonic stem (ES) cells, which were derived from C57BL/6 strain[22] by electroporation. Resultant homologous recombinant clones were isolated after G418 selection. Homologous recombination occurred on the ES clones and was confirmed by Southern blot analysis. The confirmed ES cells were then used to create chimeric mice carrying ES-derived germ cells. The chimeric mice were mated with C57BL/6J mice to obtain *B3gnt7* heterozygous mice, and the heterozygote mice were intercrossed to produce wild-type (WT; $B3gnt7^{+/+}$), heterozygous ($^{+/-}$), and null ($^{-/-}$) mice. *B3gnt7* heterozygous mice were also mated to C57BL/6J mice to maintain the strain. All procedures were approved by the Committee for Animal Experiments at Kansai Medical University, conducted according to the Guideline for Animal Experimentation at Kansai Medical University, and treated in accordance with the ARVO Statement for the Use of Animals in Ophthalmic and Vision Research.

Corneal Thickness Assay

Excised eyes of 32 mice (12- to 16-week-old mice of both sexes, 5 WT, 10 htz, and 17 null) were embedded in Tissue-Tek OCT compound (Sakura Finetek, Tokyo, Japan) and immediately frozen by dry ice. Axial whole eye sections (4 μm) were taken using Kawamoto's film method.[23] It was inferred that the sections were central and suitable for analysis when pupil

diameter was at its maximum and the optic nerve was present in the section. Unstained central corneal sections were then directly observed using phase-contrast mode of an All-in-One Microscope BZ-9000 (Keyence, Osaka, Japan). Thickness of the central cornea, stroma, and epithelium was analyzed using a measurement module of the microscope, which quantifies distance between two parallel lines. A mean value of each section was calculated from three measurements per section. Statistical analysis of thicknesses was performed by 1-way ANOVA with Dunnett's post hoc test. $P < 0.03$ compared with WT was considered significant.

Western Blot

Protein Extraction. Ten corneas from each group were minced manually using a scalpel and placed in extraction solution containing 4 M guanidine hydrochloride (Gu-HCl); 50 mM Tris/hydrochloride (Tris/HCl), pH 8.0; 10 mM EDTA; 1 mM PMSF; and 1× protease inhibitor cocktail (Nacalai Tesque, Kyoto, Japan). The protease inhibitor cocktail was diluted from a 100× stock, comprised of 50 mmol/L 4-(2-aminoethyl) benzenesulfonyl fluoride hydrochloride (AEBSF), 15 μmol/L aprotinin, 100 μmol/L E-64, and 100 μmol/L leupeptin hemisulfate monohydrate. Corneal tissue was physically pulverized using a benchtop homogenizer (Polytron 1600 E with PT-DA 1605 blade; Kinematica AG, Luzern, Switzerland) and then incubated 48 hours with rotation at 4°C in extraction solution (above). Following extraction, samples were centrifuged to separate debris in the pellet from extracted protein in the supernatant solution; the supernatant was then dialyzed in 1 L 6 M urea with 50 mM Tris/HCl (pH 8.0). The dialysis solution was refreshed at 4 hours of incubation, after which dialysis was continued overnight at 4°C with agitation. Resultant protein solutions were again centrifuged to remove debris and then concentrated by centrifugation in centrifugal filter units (Amicon Ultra-4, pore size: 30 kDa; Merck Millipore, Cork, Ireland) at 4°C and 2330*g*. Protein concentration of each extract was determined using the Pierce BCA Protein Assay kit (Pierce Biotechnology, Rockford, IL, USA) after dilution of the sample solutions with water to minimize interference of urea. Bovine serum albumin (BSA) was used to set a standard curve. All samples were measured in duplicate.

PNGase F Digestion. Peptide-N-glycosidase F (PNGase F) was used to determine whether the production of lumican core protein was affected in the heterozygous and homozygous *B3gnt7*-null mice. PNGase F cleaves KS-GAGs at the linkage GlcNAc residue, separating KS-GAGs from their lumican protein cores. Protein extracts from WT, htz, and null corneas were precipitated using a 4:1 ratio of methanol/chloroform[24] as follows. A volume of corneal extract equal to 30 μg protein was brought to 100 μL using distilled water. Ice cold methanol (400 μL) was added to the protein sample; the mixture was vortexed briefly and centrifuged to collect the solution in the base of the tube. Chloroform (100 μL) was then added to the protein/methanol mixture; the new solution was again vortexed briefly and collected into the base of the tube via centrifugation. Distilled water (300 μL) was subsequently added to the protein/methanol/chloroform mixture, vortexed thoroughly (~30 seconds), and centrifuged for 2 minutes at 20,000*g*. Following centrifugation, a protein wafer appeared at the interface of the upper aqueous and lower organic layers. After removal of the upper aqueous layer, an additional 300 μL ice-cold methanol was added to the protein sample. Thorough vortexing was conducted for ~10 seconds, and the new mixture was subjected to 20,000*g* centrifugation. The protein pellet appeared at the base of the tube, so the supernatant was removed, and the pellet was allowed to air dry before resuspending in 20 μL 1% SDS. Protein contents were measured again using the Pierce BCA Protein Assay Kit before PNGase-F digestion. PNGase-F treatment was performed by following the protocol of the company (New England Biolabs, Ipswich, MA, USA). In brief, a volume equaling 5 μg resuspended protein was denatured at 100°C for 10 minutes in manufacturer-provided glycoprotein denaturing buffer. Manufacturer-provided reaction buffer and NP-40 solution, which allows PNGase F activity in the presence of SDS, were added to denatured samples. Digestion was achieved by addition of 1 μL PNGase F (100 U/μg protein) at 37°C overnight. Digested samples were directly analyzed using SDS-PAGE and Western blot.

Endo-β-Galactosidase Digestion. To gain insight into the KS structure of htz and null corneas, endo-β-gal-ase was used. Five micrograms corneal extract was precipitated from the extraction solution (see Protein Extraction section) with methanol/chloroform as described in the PNGase F Digestion section and resuspended in 1% SDS. Resuspended solution was diluted and adjusted to 100 μL 50 mM sodium acetate, pH 6.5, 0.1% Triton X-100, and 1× proteinase inhibitor cocktail. Then, 0.5 milliunits of endo-β-gal-ase was added (0.1 mU/μg protein) and allowed to incubate overnight at 37°C with rotation. The protein samples were subsequently precipitated with methanol/chloroform as described above and were resuspended in electrophoresis sample buffer, described in the next section.

Electrophoresis. Five micrograms protein was prepared for Western blotting from untreated, PNGase F- and endo-β-gal-ase–digested samples. Samples were adjusted to 60 μL containing 1× NuPAGE LDS sample buffer and 1× reducing agent (Thermo Fisher Scientific, Rockford, IL, USA) and were denatured by boiling and then loaded into a 4% to 12% Bis-Tris polyacrylamide gel (Thermo Fisher Scientific). Constant voltage (200 V) was applied for 45 minutes or until samples reached the bottom of the gel. Immediately after electrophoresis, protein samples within the acrylamide gel were transferred to a PVDF membrane by electroblotting at 30 V for 1 hour. Blocking the protein-laden membrane was achieved at room temperature using 5% skimmed milk for 1.5 hours. Goat polyclonal anti-lumican primary antibody (R&D Systems, Minneapolis, MN, USA) was diluted 1:1000 in 5% skimmed milk and applied to the membrane for 1 hour. PBS with 0.1% Tween-20 (PBS-T) was used to rinse excess antibody from the membrane (3×, 5 minutes each). Horseradish peroxidase–conjugated secondary antibody (Santa Cruz Biotechnology, Santa Cruz, CA, USA), which recognized goat IgG, was diluted 1:2000 in 5% skimmed milk and applied to the membrane surface for 1 hour. To develop the membranes, Chemi-Lumi One chemiluminescence substrate (Nacalai Tesque) was applied to the membrane for 2 minutes. Chemiluminescent images were captured using LAS 3000 Mini camera and software (Fuji Photo Film, Tokyo, Japan) using 1 to 10 minutes of exposure, depending on the amount of signal produced by the membrane.

Electron Microscopy

Whole corneas from WT, htz, and null mice were excised and immediately prefixed in 4% paraformaldehyde in 0.1 M Sorensen phosphate buffer (pH: 7.4) for 10 minutes. After initial fixation, excess prefixative was rinsed with 1× Tris-acetate buffer, and whole corneas were further dissected into quarters. "Untreated" (i.e., not subjected to chondroitinase ABC or buffer reaction conditions) corneal quarters were immediately placed into 2.5% (w/v) glutaraldehyde (Agar Scientific Ltd., Stansted, United Kingdom) in 25 mM sodium acetate buffer (pH 5.7) with 0.05% cupromeronic blue (w/v) (Sigma, St. Louis, MO, USA) and magnesium chloride ($MgCl_2$) at critical electrolyte concentration, 0.1 M—a concentration

known to enhance PG staining.[25,26] To allow for KS visualization, remaining corneal quarters from each genotype were digested with chondroitinase ABC for 4 hours at 37°C in the following reaction mixture: 1 μg/mL chondroitinase ABC was added to 1× Tris-acetate buffer + bovine serum albumin (pH 8), including 10 μl/mL general protease inhibitor. Samples were subjected to constant agitation for the duration of the reaction. Following incubation, specimens were rinsed in 25 mM sodium acetate buffer containing 0.1 M $MgCl_2$ and further fixed/stained overnight at room temperature on a rotator in the cupromeronic blue solution described above. One corneal quarter from each group was also processed in buffer solution lacking chondroitinase ABC as a control. Fixed and stained specimens (untreated, chondroitinase ABC digested, and buffer treated) were washed three times (10 min/wash) in 0.5% (w/v) sodium tungstate (Sigma) and then dehydrated using an ascending series of ethanol solutions (70% to 100%) for 15 minutes each. Propylene oxide (Agar Scientific Ltd.) was used as a transition solvent between ethanol and resin steps by washing dehydrated samples twice in 100% propylene oxide (15 min/wash), followed by incubation in a 1:1 mixture of propylene oxide and resin for 1 hour. Six changes, approximately 3 hours each, of Araldite resin (CY212 monomer; Taab Laboratories, Aldermaston, United Kingdom) containing dodecenylsuccinic anhydride (DDSA) hardener (Agar Scientific Ltd.) and benzyl di-methyl amine (BDMA) accelerator (Agar Scientific Ltd.) ensured total removal of residual propylene oxide and complete infiltration of resin into each specimen block. Samples were then transferred to molds and polymerized for a minimum of 24 hours at 60°C. Ultrathin sections (~90 nm) were created using a Leica UC6 ultramicrotome (Leica Microsystems (UK) Ltd., Milton Keynes, United Kingdom) equipped with a diamond knife. Sections were collected on copper grids (3.05 mm) and stained for 30 minutes with a saturated uranyl acetate solution for added collagen contrast, followed by three rinses in 0.2-μm filtered distilled water (5 min/rinse). Sections were allowed to dry and examined using a JEOL 1010 transmission electron microscope (Jeol (UK) Ltd., Welwyn Garden City, United Kingdom) operating at 80 kV.

Immunofluorescence

WT and null whole mouse eyes were harvested fresh, embedded in OCT compound, frozen on dry ice, and stored at −80°C. Whole-eye cryosections 10 μm thick were collected on poly-lysine–coated glass slides (Fisher Scientific, Loughborough, United Kingdom), using a Bright OTF5000 cryostat (Bright Instruments Ltd., Luton, United Kingdom). Sectioning was performed along the eye globe's sagittal plane, and sections were only kept for analysis if the iris was disconnected, indicating corneal tissue was centrally located over the pupil. To prevent nonspecific background labeling between anti-mouse secondary antibody and IgG native to mouse corneal tissue, primary and secondary antibodies were incubated overnight at 4°C with constant rotation in the following reaction mixture: primary and secondary antibodies were diluted 1:10 and 1:50, respectively, in 1× PBS with 0.1% Tween-20 and 2% BSA (PBS-T+BSA).[27,28] This preincubation facilitated the interaction between secondary antibodies and the Fc region of primary antibodies, minimizing erroneous localization of secondary to murine corneal sections. For 30 minutes prior to tissue application, heat-deactivated normal mouse serum was added to antibody and control mixtures at a concentration of 5 μL/μg secondary antibody to bind potentially free secondary antibody (further reducing background labeling). Rehydration of sections was achieved by applying PBS-T for 5 minutes. Sections were immersed for 30 minutes in 1% Triton X-100 in PBS to further reduce background fluorescence. Sections were briefly rinsed in PBS-T prior to blocking or, in some cases, application of the keratanase or chondroitinase ABC enzymes. When applied, both keratanase and chondroitinase ABC were prepared at a 0.4 U/mL concentration in either 10 mM Tris-HCl (keratanase) or 50 mM Tris and 60 mM sodium acetate with 0.02% BSA (chondroitinase ABC); digestion occurred for 2 hours at 37°C in both cases. Sections were rinsed with PBS-T following enzyme incubation (where applicable) and blocked for 30 minutes with 10% (v/v) normal goat serum in PBS-T+BSA. Finally, tissue sections were covered in a generous volume of the antibody mixture for 4 hours at room temperature in a humid atmosphere. Following application of primary-secondary complexed antibody solutions, sections were thoroughly washed with PBS-T and mounted with Vectashield dual mountant and 4′,6-diamidino-2-phenylindole (DAPI) stain. Control solutions were prepared as described above, except PBS-T+BSA buffer replaced the volume of the primary antibody. Slides were stored at 4°C for no more than 24 hours before imaging as described below. Images were collected with an Olympus BX40 fluorescence microscope equipped with an SIS F-View black and white digital camera (Olympus Keymed Ltd., Southend-on-Sea, United Kingdom). Olympus Cell^P imaging software (Olympus Keymed Ltd., Southend-on-Sea, United Kingdom) was used to capture images in TIFF format.

Results

B3gnt7-Null Mouse Phenotype

Intercross of *B3gnt7* heterozygotes produced WT, htz, and null mice at normal Mendelian frequency. *B3gnt7*-null mice were born without any detectable abnormalities and were indistinguishable from WT and *B3gnt7*-htz littermates during development from neonate to adult stages, indicating neither abnormalities nor major visible phenotypes arise from *B3gnt7*-null mutation. A 1-year follow-up study showed that *B3gnt7*-null mutations were nonlethal, and mice maintained normal development, lacking any overt abnormalities. Intercross of null mice produced litters of comparable size to those of intercrossed WT mice, indicating that the mutant mice have normal reproductive potential.

Corneal Thickness

Thickness measurements of the whole cornea, the collagen-rich corneal stroma, and the corneal epithelium in WT, *B3gnt7*-htz, and *B3gnt7*-null eyes were collected (Fig. 2). Dimensions of the cornea were comparable in WT and htz tissue, with the epithelium measuring 34 ± 1 vs. 33 ± 1 μm, the whole cornea measuring 109 ± 2 vs. 108 ± 3 μm, and the stroma measuring 75 ± 2 vs. 75 ± 3 μm (all comparisons WT versus htz). None of these small differences were statistically significant. Corneal epithelial thickness in the *B3gnt7*-null mouse, at 32 ± 1 μm, also showed no statistical differences ($P = 0.4702$ and $P = 0.8898$, respectively) to the epithelial thickness measurements of the WT or htz corneas. In contrast, a noteworthy decrease in corneal stromal thickness in *B3gnt7*-null mouse eyes, measured at 60 ± 2 μm, was noted. This measurement was less than the corresponding values for the WT and htz corneal stromas (75 ± 2 and 75 ± 3 μm, respectively; $P = 0.0024$ and $P = 0.0002$). Given that the epithelial thicknesses in each of the three genotypes was unaltered, the reduction in stromal thickness was reflected in the whole cornea thickness measurements. The *B3gnt7*-null whole cornea was thinner than WT and htz corneas (93 ± 2 vs. 109 ± 2 and 108 ± 3 μm, respectively: $P = 0.0011$ and $P = 0.0002$).

Investigative Ophthalmology & Visual Science

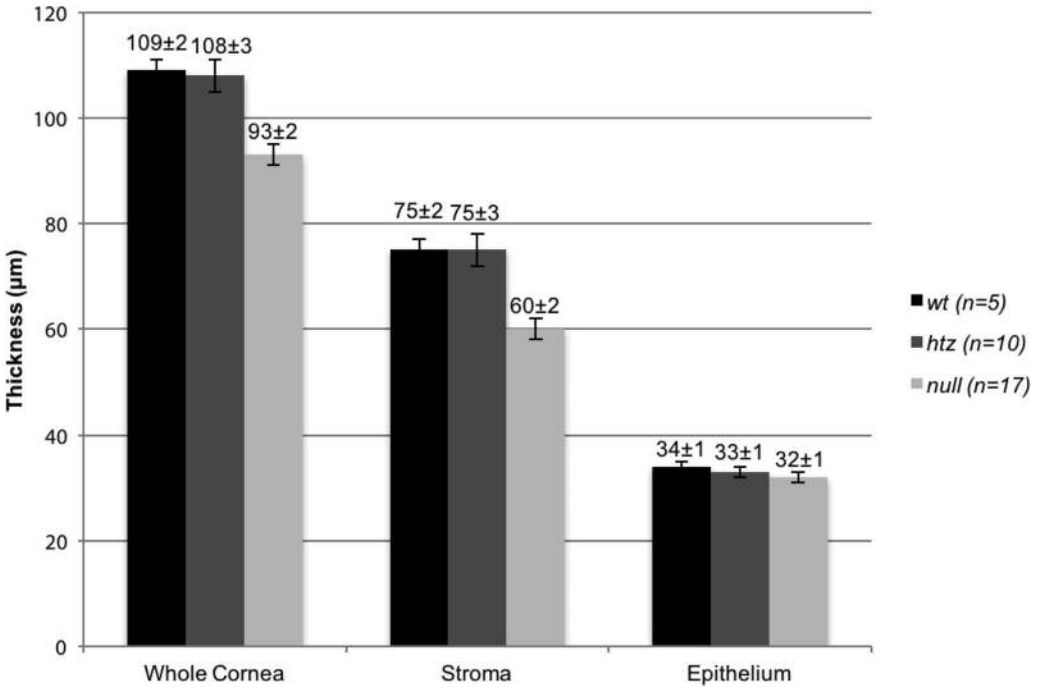

Figure 2. Whole cornea, stromal, and epithelial thicknesses of WT, *B3gnt7*-htz, and null tissue. WT (*black bars*) and htz (*dark gray bars*) measured similarly, with whole cornea thicknesses of 109 ± 2 vs. 108 ± 3 μm and stromal thicknesses of 75 ± 2 vs. 75 ± 3 μm. Stromal, and therefore whole cornea, thickness of *B3gnt7*-null (*light gray bars*) tissue was significantly thinner than those of the WT and htz, measuring 60 ± 2 and 93 ± 2 μm, respectively. This result contrasted with epithelial thicknesses, where WT, htz, and null measured 34 ± 1, 33 ± 1, and 32 ± 1 μm, respectively.

KS Chain Length, Lumican Production, and Galactose Sulfation

KS-chain length, lumican expression, and galactose sulfation patterns in WT, htz, and null tissues were investigated using extracted corneal protein for Western blot analyses. Three samples were prepared for each genotype: untreated, PNGase F digested, and endo-β-galactosidase digested. The untreated samples, prepared to determine intact KS-GAG chain length as a function of the rate at which lumican migrated through the electrophoretic gel, revealed that WT and htz produced similar high-to-low molecular weight smear patterns, ranging from ~160 to 45 kDa (Fig. 3, lanes 1 and 2, respectively). In contrast, *B3gnt7*-null corneal extracts showed a more condensed band from ~65 to 45 kDa (Fig. 3, lane 3), suggesting that lumican from *B3gnt7*-null extracts may be substituted with lower-molecular-weight (i.e., shorter) KS-GAGs compared with WT or htz samples. To confirm that this finding was a consequence of KS-GAG chain length, PNGase F was used to cleave KS side chains from their lumican core proteins. After PNGase F predigestion, all three samples showed identical narrow bands at ~40 kDa (Fig. 3, lanes 4–6), which corresponds to the known molecular weight of lumican, ~36 to 40 kDa.[29] Endo-β-galactosidase (endo-β-gal-ase) treatment was used to probe for aberrant galactose sulfation of KS-GAGs, as its cleavage site is the β-1,4 glycosidic linkage between unsulfated galactose and GlcNAc (sulfated or unsulfated).[30] It should be noted that endo-β-gal-ase will cleave at each unsulfated galactose along KS-GAGs, leaving lumican core proteins bound to the KS linkage region and GAG stub proximal to the innermost unsulfated galactose. Therefore, because WT, htz, and null samples that were digested with this enzyme produced bands of comparable molecular weight and density at ~47 kDa (Fig. 3, lanes 7–9), it was inferred that the innermost unsulfated galactose was not atypically oversulfated in *B3gnt7*-htz and -null mutants. Whether or not galactose residues in the non-reducing terminal region of KS are affected by the *B3gnt7* mutation remains unknown.

Electron Microscopy: Tissue Architecture

Corneal tissue was examined by electron microscopy at high magnification such that aligned collagen fibrils were oriented in longitudinal section. Visualization of polyanionic PG structures was achieved via the inclusion of cupromeronic blue in the primary fixative.[25,31] Because cupromeronic blue binds the two major families of PGs native to the corneal stroma—CS/DS-PGs and KS-PGs—chondroitinase ABC was required to distinguish CS/DS from KS in electron micrographs. Tissue from all three groups was either left intact (Fig. 4, left column) or subjected to chondroitinase ABC (Fig. 4, right column), an enzyme that hydrolyzes glycosidic linkages within the core structure of CS/DS-GAGs[32,33] without affecting KS-PGs. It should be noted that heparan sulfate, a third class of PGs, is also present in corneal tissue, albeit at much lower levels in the stroma than either KS- or CS/DS-PGs.[34] Chondroitinase ABC preincubation was therefore sufficient for distinction between the two major classes of stromal PGs.

Non–enzyme-treated WT corneas showed many electron dense structures extending perpendicularly from collagen fibril axes, which sometimes appeared to associate with collagen at consistent distances (Fig. 4a, white asterisks). Occasionally, longer filaments traversing through or aligning with collagen fibrils were identifiable (Fig. 4a, black arrows). Very fine, short strands of low contrast were also observed projecting outward from collagen fibril axes (Fig. 4a, black arrowhead) throughout the untreated WT stroma. Non–enzyme-treated *B3gnt7*-htz tissue (Fig. 4c) presented phenotypically similar to the WT tissue, with numerous electron dense structures associating with collagen in parallel and perpendicular fashions (Fig. 4c,

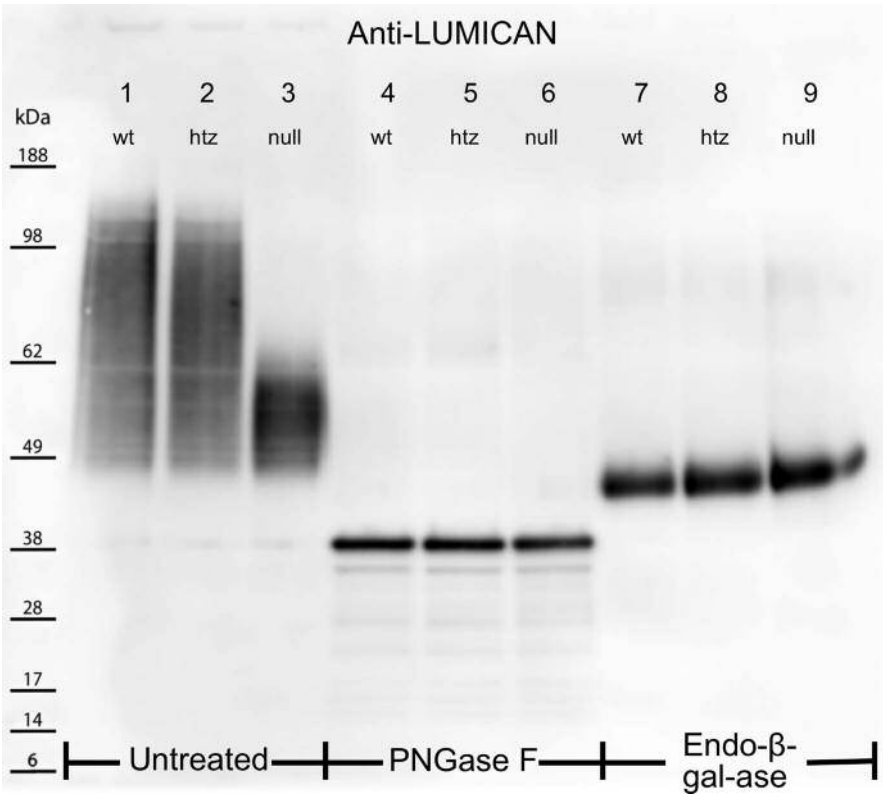

Figure 3. Electrophoretically separated untreated (lanes 1–3), PNGase F– (lanes 4–6), and Endo-β-Gal-ase–digested (lanes 7–9) corneal extracts were probed for the KS core protein, lumican. Untreated WT and htz samples produced smear patterns from ~160 to 45 kDa (lanes 1, 2), whereas untreated null extracts showed a more condensed band from 45 to 65 kDa (lane 3). PNGase F cleaved KS-GAG chains from lumican core proteins in lanes 4–6. The migration of lumican into narrow, low-molecular-weight bands at 40 kDa for all three samples indicated the differential smear patterns in the untreated samples were a result of altered KS structures. Lanes 7–9 show lumican localization following cleavage of KS-GAGs at unsulfated Gal residues using Endo-β-Gal-ase. All three samples showed thick bands at ~46 kDa following this treatment, suggesting sulfation of Gal residues is unaffected by the *B3gnt7* mutation.

black arrows). Polyanionic structures observed in untreated *B3gnt7*-null tissue appeared several-fold longer than those in WT or htz samples and contained many filamentous offshoots extending perpendicularly from their axes (Fig. 4e, white arrowheads). Critical measurements for accurate comparison of PG length were not possible without three-dimensional imaging, owing to the tortuous course of these structures, which ramified in and out of the plane of the ultrathin section. Additionally, whereas most of the PGs found in WT specimens in this study associated orthogonally to collagen fibrils, the structures prevalent in the null specimen mainly aligned parallel to fibril axes.

Compared with their untreated counterparts shown in the left column of Figure 4, overall GAG content visibly decreased in all specimens following chondroitinase ABC digestion (Fig. 4, right column). Black arrowheads in Figures 4b and 4d identify residual short strands, thought to be KS-PGs owing to their chondroitinase ABC resistance, found throughout the stroma in WT and htz samples (Figs. 4b, 4d, black arrowheads).[14,35] Interestingly, *B3gnt7*-null corneal specimens did not feature polyanionic structures following chondroitinase ABC digestion, suggesting an atypical absence of KS in circumstances where both alleles of *B3gnt7* were mutated. Additionally, the irregular PGs found throughout the untreated null sample were totally eliminated from the null corneal stroma upon chondroitinse ABC preincubation, suggesting the anomalous PGs were elongated electron-dense CS/DS-PG filaments.

The cupromeronic blue-enhanced PG phenotypes discussed here were similar at anterior, middle, and posterior stromal depths, as was collagen fibril diameter. No aberrantly thick or thin collagen fibrils were observed in any of the genotypes or stromal regions studied (data not shown). Finally, corneal tissue that was incubated in buffer-maintained morphology and proteoglycan content comparable to non–enzyme-treated tissue, confirming that diminished PG content was dependent on active chondroitinase enzyme.

Immunofluorescence: Confirming the KS and CS/DS Phenotypes

The mouse monoclonal antibody 1B4, which is specific for low sulfated KS,[36] was applied to cryosections of WT and null corneas to localize KS-GAGs. Traditionally, detection of highly sulfated KS is achieved with 5D4, a mouse monoclonal antibody with specificity for KS hexasaccharides with a minimum of five sulfate moieties.[37,38] However, previous work has demonstrated the 5D4 epitope is not present in mouse corneal tissue at a concentration sufficient for immunofluorescent labeling.[35] As such, we instead probed samples with 1B4 to visualize low sulfated KS. Figure 5a shows the WT corneal stroma was diffusely fluorescent when probed for sulfated KS-GAGs. Additionally, brightly punctate fluorescence was discernible at various stromal depths (Fig. 5a, white arrows). These results contrasted with null tissue, which showed only faint epithelial staining juxtaposed to a dark stroma (Fig. 5e).

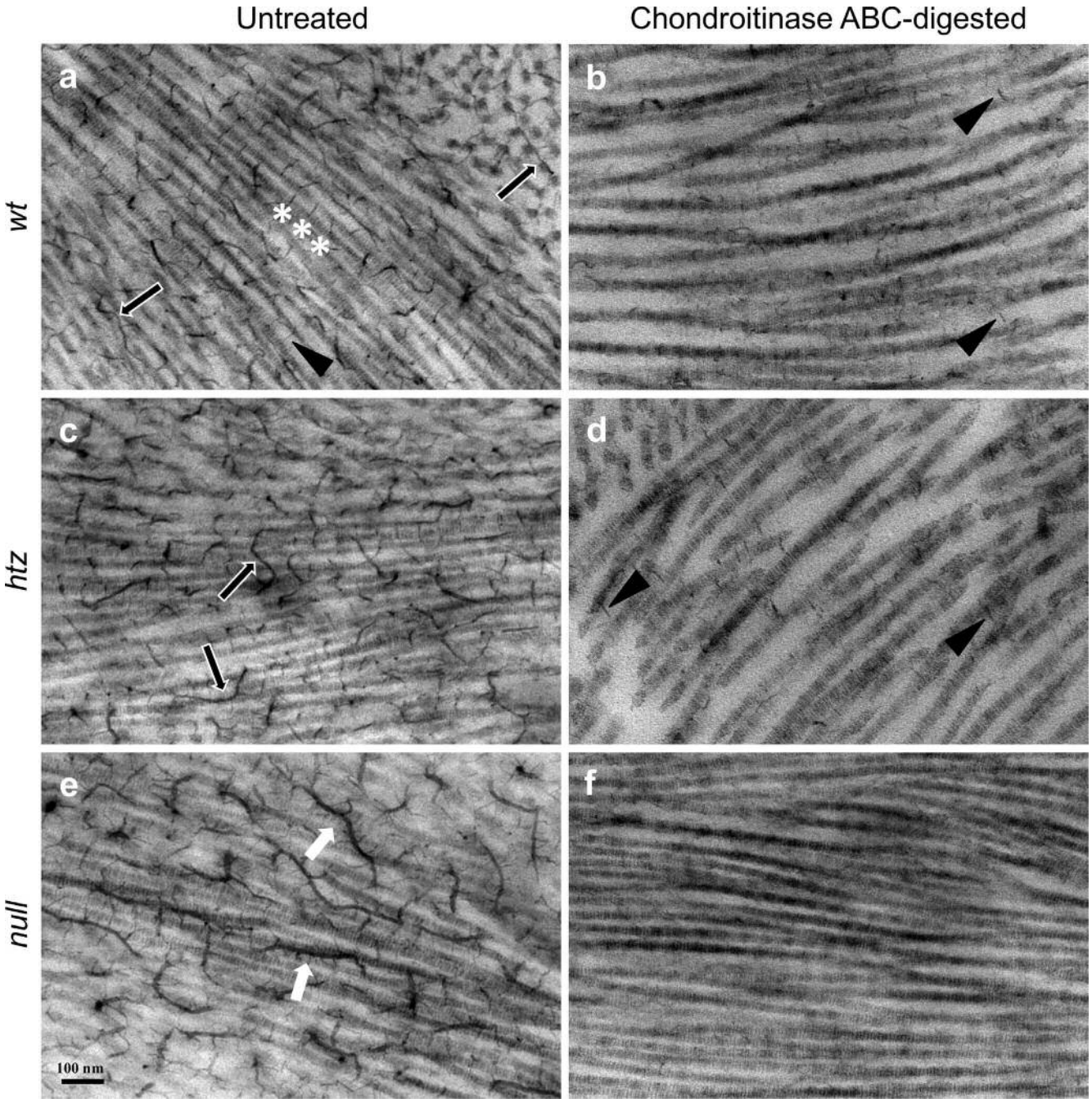

Figure 4. Electron micrographs of untreated (**a**, **c**, **e**) and chondroitinase ABC-digested (**b**, **d**, **f**) WT, htz, and null corneal stromal tissue. All images show striated collagen fibrils running in longitudinal section. Putative CS/DS-PGs (*black arrows*, **a**, **c**) were observed throughout the stroma of untreated WT (**a**) and htz (**c**) corneal tissue and sometimes associated with collagen fibrils at regular intervals (*white asterisks*, **a**). KS-PGs appeared shorter and projected outward to the next nearest collagen fibril in untreated WT tissue (*black arrowhead*, **a**). Untreated null specimens (**e**) possessed markedly elongated, branched PG filaments (*white arrows*) that were not seen in WT or htz samples. In all three groups, overall PG content decreased on chondroitinase ABC preincubation, although only the WT and htz (**b**, **d**, respectively) specimens contained residual short chain KS-PGs (*black arrowheads*). The lack of any discernible PGs following enzymatic digestion in the null (**f**) samples suggested an abnormal KS-PG phenotype, arising from defunct β3GnT7. All images were taken at 20,000× magnification. *Scale bar* denotes 100 nm.

Figures 5b and 5d represent tissue sections that were subjected to keratanase digestion before immuno-labeling for KS. Because stromal fluorescence in the WT was abolished following keratanase predigestion, it was inferred that the signal observed in the undigested WT tissue was indeed due to specific labeling of KS-GAGs.

Immunofluorescence was also used to detect possible changes in CS/DS content of the null corneal stroma compared with WT tissue. To this end, 2B6 antibody, which requires chondroitinase ABC predigestion to reveal the chondroitin-4-sulfate and DS epitopes,[36,39,40] was applied to corneal sections. Both WT (Fig. 5c) and null (Fig. 5g) specimens produced fluorescent signal through the depth of the cornea. The null specimen displayed slightly stronger signal compared with the WT, perhaps reflecting the appearance of the distinctively elongated family of electron dense PG filaments observed in

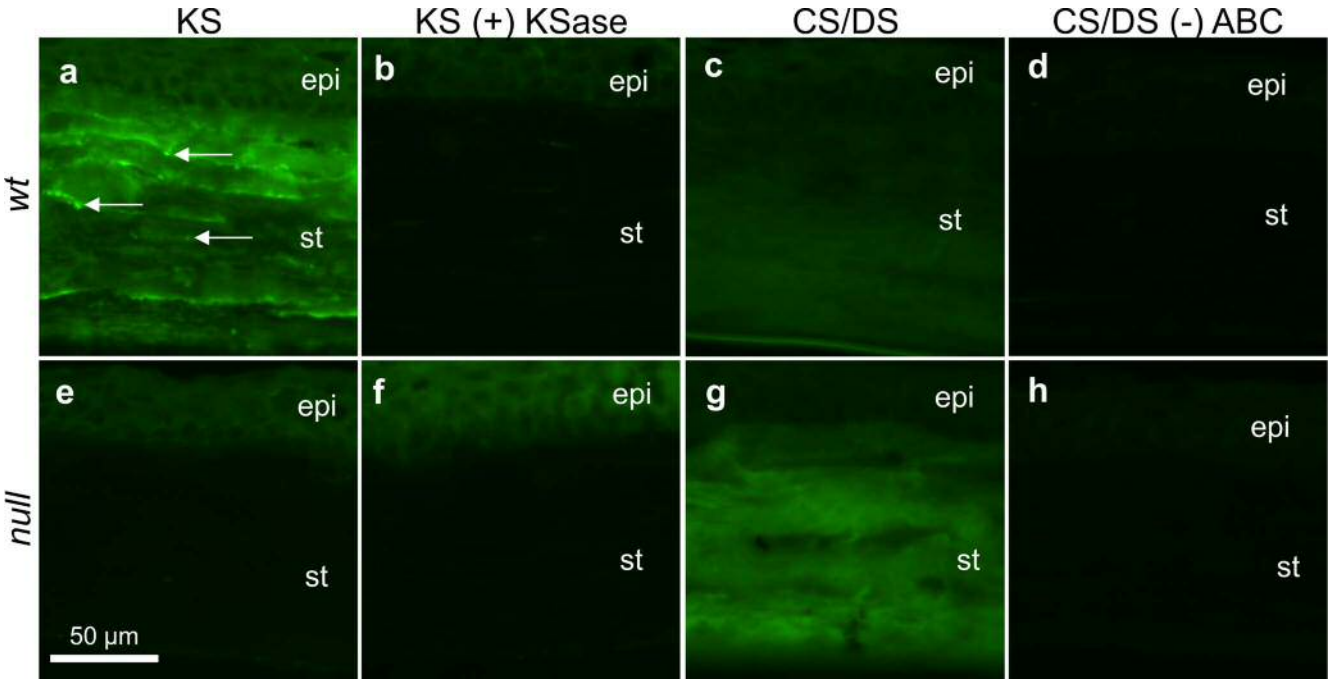

Figure 5. Immunofluorescent labeling of low-sulfated KS- and CS/DS-GAGs in WT (**a**–**d**) and null (**e**–**h**) corneal tissue. WT tissue labeled for KS-GAGs fluoresced at all stromal depths and featured occasional bright punctae (*white arrows*, **a**); this signal was sensitive to keratanase (KSase) digestion (**b**). The lack of fluorescent signal in the null corneal stroma, without (**e**) or with (**f**) KSase incubation, implied a lack of sulfated KS-GAGs in the mutated corneal stroma. Chondroitinase ABC-liberated CS/DS-GAG "stubs" were local to WT (**c**) and null (**g**) tissue throughout the depth of the corneal stroma. A brighter stromal fluorescent signal from the null specimen, relative to the WT control, indicated increased CS/DS content in the *B3gnt7* knockout. In absence of chondroitinase ABC predigestion, neither WT (**d**) nor null (**h**) tissue appeared positive for the 2B6 stub epitope. Epi, corneal epithelium; st, stroma. All images were collected at 40× magnification. *Scale bar* denotes 50 μm.

electron micrographs. The 2B6 antibody was also applied to sections without revealing the epitope via chondroitinase ABC predigestion as a form of negative control. As expected, neither WT nor null (Figs. 5d, 5h, respectively) corneas exhibited positive fluorescence under these conditions.

Discussion

The work presented here revealed for the first time a relationship between β3GnT7 and the KS-PG phenotype in murine corneal tissue. Our findings, discussed below, demonstrated that an abnormally attenuated *B3gnt7*-null mouse corneal stroma lacked histochemically detectable KS-PGs. The concurrent appearance of elongated, branched electron dense PG filaments in this knockout mouse, which were susceptible to chondroitinase ABC, perhaps preserved corneal ultrastructure in absence of typical KS-PGs.

Because in vitro work by Kitayama et al.[17] identified β3GnT7 as a key enzyme in KS-GAG elongation, we hypothesized that KS-PGs would be altered in the *B3gnt7*-null tissue, thereby affecting overall corneal architecture. Lumican from *B3gnt7*-null corneas appeared to be modified with shorter carbohydrate chains than those from WT and *B3gnt7*-htz corneas (Fig. 3), indicating that β3GnT7 is a major enzyme contributing to corneal KS-GAG synthesis. This is consistent with previously published in vitro observations. Endo-β-gal-ase digestion shortened carbohydrate chains on lumican protein cores in WT, *B3gnt7*-htz, and null corneas, the resulting structures of which appeared to contain short remnants of either poly-*N*-acetyllactosamine or KS-GAGs. There are eight β1,3-GlcNAc transferases in mice, and both β-1,3-*N*-acetylglucosaminyltransferase-2 (β3GnT2) and β3GnT7 have been shown to act on KS-GAG synthesis in vitro.[17,18] Thus, it is possible that β3GnT2 may work on KS-GAG chain production to compensate for lack of β3GnT7 in *B3gnt7*-null corneas. Although, if β3GnT2 participates in KS biosynthesis, its action is apparently insufficient to fully elongate KS-GAGs in absence of β3GnT7. Future studies should determine whether these results are reflected in all KS-PG core proteins, including keratocan and mimecan, because we analyzed lumican KS-PGs as a representative carrier of KS-GAGs in the mouse cornea.

We believe the widespread disappearance of KS-PGs from EM and fluorescence images of the affected null corneas, but not in the WT, supports the idea that the biosynthetic mechanism underlying KS-PG synthesis was disrupted in cases where both alleles of *B3gnt7* were deactivated (Fig. 6). These results confirmed predictions of in vitro work, despite the biosynthesis environment in vivo differing. Whereas in vitro studies were conducted with solubilized enzymes and synthetic oligosaccharide constructs,[18] in vivo glycosyltransferases and sulfotransferases are membrane-bound enzymes within Golgi compartments. Indeed, it is as yet unconfirmed whether or not these glycosyl- and sulfotransferases share Golgi compartments in keratocytes, allowing them to act in tandem as hypothesized. That said, highly sulfated KS was detected in culture media of human corneal epithelial cells that were modified to express both CGn6ST and KSGal6ST, perhaps complementing their endogenously expressed β3GnT7 and β4GalT4.[17] The consistent importance of β3GnT7 in in vitro, and now in our in vivo, assays provides strong evidence for the participation of β3GnT7 in corneal KS-GAG synthesis.

Architecture of the *B3gnt7*-null mouse cornea emulates stromal changes characteristic of human macular corneal dystrophy (MCD) and *Chst5*-null mouse tissue, both of which lack properly sulfated KS throughout the corneal matrix. Corneal phenotypes in both human MCD and murine *Chst5*-null present with a ~20% reduced stromal thickness,[14,41] an

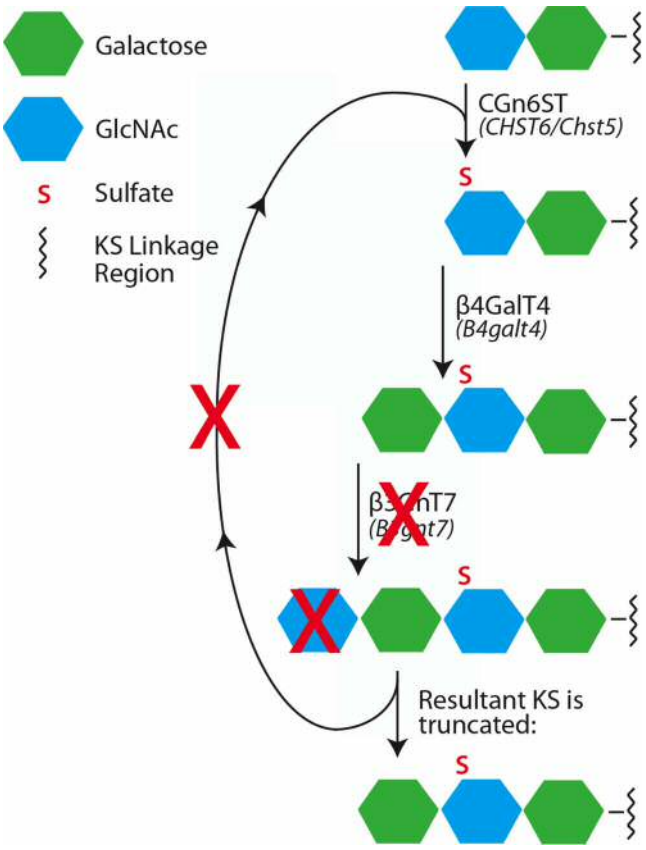

Figure 6. Hypothesized KS biosynthetic pathway in the absence of functional β3GnT7. We hypothesize that without operative β3GnT7, GlcNAc cannot be added to its Gal substrate (shown by a *red X* over GlcNAc) to form the KS repeating disaccharide. Without a terminal GlcNAc residue, perhaps the catalytic addition of Gal, GlcNAc, and sulfate cannot repeat as normal (*red X* over *arrowed loop*), resulting in an atypically shortened KS structure.

attenuation equivalent to the amount of stromal thinning observed in the *B3gnt7*-null specimen in our corneal thickness assay (Fig. 2). Interestingly, human *CHST6* and murine *Chst5* mutations result in deactivation of human CGn6ST and the analogous mouse intestinal GlcNAc-6-*O*-sulfotransferase, respectively, without which the KS-GAG biosynthetic pathway cannot proceed. Because all three of these cases—*B3gnt7*-null, MCD, and *Chst5*-null—result in abnormally short KS-GAG chains and experience similar levels of stromal thinning, we propose that this consistent phenotype results from decreased water retention within the stroma, arising from a deficiency in water sorptive KS-PGs.[42,43] The ultrastructural basis for the thin cornea in MCD is believed to be a closer-than-normal packing of the uniformly thin collagen fibrils, which make up the bulk of the corneal stroma.[9] This is thought to arise from a reduction in water-binding potential in the extrafibrillar space, alluded to above, augmented by a lack of mutual repulsion between charged KS side chains on KS-PGs, whose protein cores are bound to collagen fibrils. Indeed, this concept finds some support in depth-profiled studies of collagen fibril spacing in human MCD corneas, which show that the compaction of collagen fibrils is more prevalent in the posterior corneal stroma,[9,44] a region of the tissue in mammalian corneas in which KS-GAGs are most abundant.[45–47] Reduction in center-to-center distance between collagen fibrils was observed in x-ray diffraction studies of *Chst5*-null corneal tissue,[14] further demonstrating a role for KS-PGs in maintenance of interfibrillar spacing. The relatively thin corneal stroma of the *B3gnt7*-null specimen perhaps arises from a comparable change in collagen packing, although this hypothesis should be demonstrated empirically in future publications.

In addition to the anomalous KS-PG phenotype discovered in the *B3gnt7*-null cornea, a concomitant appearance of uniquely elongated, branched electron dense PG filaments was found when corneas were examined using electron microscopy. The susceptibility of these PGs to chondroitinase ABC digestion indicates the atypical PGs were CS/DS in nature. Similar CS/DS structures were previously observed by electron microscopy in *Chst5*-null corneas of mice lacking keratan sulfate sulfotransferase.[15] Lateral aggregation or end-to-end aggregation of single GAGs were suggested as possible mechanisms generating these supernormal structures, and we speculate that similar processes may underlie their appearance in *B3gnt7* mutants as well. However, future work is required on this knockout to reveal the nature of the highly electron dense structures revealed by electron microscopy. That said, an argument for upregulation of CS/DS-PGs in absence of KS-PGs could be rationalized. Considering that corneal transparency partially relies on repulsion between negatively charged KS- and CS/DS-PGs,[48] it is unsurprising that upregulation of CS/DS-PGs may prevent the breakdown of collagen organization necessary for corneal clarity in the event of a charge deficit (i.e., in the absence of elongated, sulfated KS). Indeed, this compensation mechanism was posited before by Hayashida et al.,[14] whose work revealed *Chst5*-null mice formed "caterpillar-like" structures susceptible to chondroitinase ABC digestion, similar—if not, identical—to those described in this study. The possibility of a compensatory mechanism is further supported by the work of Plaas et al.,[49,50] which characterized the GAG content of normal human corneas versus those affected by MCD. Their work demonstrated that diseased tissue contained fewer sulfated KS-PGs, and CS/DS-PGs were significantly increased and were in an atypically oversulfated form.

The data within demonstrate that the GlcNAc-transferring ability of β3GnT7 is necessary for synthesis of corneal KS-GAGs and aid our understanding of the structure–function relationship between KS and corneal ultrastructural organization.

Acknowledgments

Supported by National Institutes of Health Grant EY014620 (TOA), Japan Society for the Promotion of Science (JSPS) Grant 25462741 (TOA), the Cardiff University International Scholarship (SLL, AJQ), and the Sir Martin Evans President's Research Scholarship (SLL, AJQ).

Disclosure: **S.L. Littlechild**, None; **R.D. Young**, None; **B. Caterson**, None; **H. Yoshida**, None; **M. Yamazaki**, None; **K. Sakimura**, None; **A.J. Quantock**, None; **T.O. Akama**, None

References

1. Funderburgh JL. Keratan sulfate biosynthesis. *IUBMB Life*. 2002;54:187–194.
2. Oeben M, Keller R, Stuhlsatz HW, Greiling H. Constant and variable domains of different disaccharide structure in corneal keratan sulphate chains. *Biochem J*. 1987;248:85–93.
3. Meyer K, Linker A, Davidson EA, Weissmann B. The mucopolysaccharides of bovine cornea. *J Biol Chem*. 1953; 205:611–616.
4. Funderburgh JL. Keratan sulfate: structure, biosynthesis, and function. *Glycobiology*. 200;10:951–958.
5. Tai GH, Huckerby TN, Nieduszynski IA. Multiple non-reducing chain termini isolated from bovine corneal keratan sulfates. *J Biol Chem*. 1996;271:23535–23546.

6. Nakazawa K, Hassell JR, Hascall VC, Lohmander LS, Newsome DA, Krachmer J. Defective processing of keratan sulfate in macular corneal dystrophy. *J Biol Chem*. 1984;259:13751–13757.
7. Klintworth GK, Meyer R, Dennis R, et al. Macular corneal dystrophy. Lack of keratan sulfate in serum and cornea. *Ophthalmic Paediatr Genet*. 1986;7:139–143.
8. Midura RJ, Hascall VC, MacCallum DK, et al. Proteoglycan biosynthesis by human corneas from patients with types 1 and 2 macular corneal dystrophy. *J Biol Chem*. 1990;265:15947–15955.
9. Quantock AJ, Meek KM, Ridgway AE, Bron AJ, Thonar EJ. Macular corneal dystrophy: reduction in both corneal thickness and collagen interfibrillar spacing. *Curr Eye Res*. 1990;9:393–398.
10. Young RD, Akama TO, Liskova P, et al. Differential immunogold localisation of sulphated and unsulphated keratan sulphate proteoglycans in normal and macular dystrophy cornea using sulphation motif-specific antibodies. *Histochem Cell Biol*. 2007;127:115–120.
11. Akama TO, Nishida K, Nakayama J, et al. Macular corneal dystrophy type I and type II are caused by distinct mutations in a new sulphotransferase gene. *Nat Gen*. 2000;26:237–241.
12. Liu NP, Dew-Knight S, Rayner M, et al. Mutations in corneal carbohydrate sulfotransferase 6 gene (CHST6) cause macular corneal dystrophy in Iceland. *Mol Vis*. 2000;6:261–264.
13. Akama TO, Nakayama J, Nishida K, et al. Human corneal GlcNac 6-O-sulfotransferase and mouse intestinal GlcNac 6-O-sulfotransferase both produce keratan sulfate. *J Biol Chem*. 2001;276:16271–16278.
14. Hayashida Y, Akama TO, Beecher N, et al. Matrix morphogenesis in cornea is mediated by the modification of keratan sulfate by GlcNAc 6-O-sulfotransferase. *Proc Natl Acad Sci U S A*. 2006;103:13333–13338.
15. Parfitt GJ, Pinali C, Akama TO, et al. Electron tomography reveals multiple self-association of chondroitin sulphate/dermatan sulphate proteoglycans in Chst5-null mouse corneas. *J Struct Biol*. 2011;174:536–541.
16. Seko A, Yamashita K. β1,3-*N*-Acetylglucosaminyltransferase-7 (β3Gn-T7) acts efficiently on keratan sulfate-related glycans. *FEBS Lett*. 2004;556:216–220.
17. Kitayama K, Hayashida Y, Nishida K, Akama TO. Enzymes responsible for synthesis of corneal keratan sulfate glycosaminoglycans. *J Biol Chem*. 2007;285:30085–30096.
18. Akama TO, Misra AK, Hindsgaul O, et al. Enzymatic synthesis in vitro of the disulfated disaccharide unit of corneal keratan sulfate. *J Biol Chem*. 2002;277:42505–42513.
19. Fukuta M, Inazawa J, Torii T, Tsuzuki K, Shimada E, Habuchi O. Molecular cloning and characterization of human keratan sulfate Gal-6-sulfotransferase. *J Biol Chem*. 1997;272:32321–32328.
20. Hoshino H, Foyez T, Ohtake-Niimi S, et al. KSGal6ST is essential for the 6-sulfation of galactose within keratan sulfate in early postnatal brain. *J Histochem Cytochem*. 2014;62:145–156.
21. Copeland NG, Jenkins NA, Court DL. Recombineering: a powerful new tool for mouse functional genomics. *Nat Rev Genet*. 2001;2:769–779.
22. Mishina M, Sakimura K. Conditional gene targeting on the pure C57BL/6 genetic background. *Neurosci Res*. 2007;58:105–112.
23. Kawamoto T. Use of a new adhesive film for the preparation of multi-purpose fresh-frozen sections from hard tissues, whole-animals, insects and plants. *Arch Histol Cytol*. 2003;66:123–143.
24. Wessel W, Flügge UI. A method for the quantitative recovery of protein in dilute solution in the presence of detergents and lipids. *Anal Biochem*. 1984;138:141–143.
25. Scott JE. Collagen–proteoglycan interactions. Localization of proteoglycans in tendon by electron microscopy. *Biochem J*. 1980;187:887–891.
26. Scott JE. Histochemistry of Alcian blue. *Histochem Cell Biol*. 1972;32:191–212.
27. Hierck BP, Iperen LV, Gittenberger-De Groot AC, Poelmann RE. Modified indirect immunodetection allows study of murine tissue with mouse monoclonal antibodies. *J Histochem Cytochem*. 1994;42:1499–1502.
28. Goodpaster T, Randolph-Habecker J. A flexible mouse-on-mouse immunohistochemical staining technique adaptable to biotin-free reagents, immunofluorescence, and multiple antibody staining. *J Histochem Cytochem*. 2014;62:197–204.
29. Kao WW, Funderburgh JL, Xia Y, Liu CY, Conrad GW. Focus on molecules: lumican. *Exp Eye Res*. 2006;82:3–4.
30. Fukuda MN. Purification and characterization of endo-beta-galactosidase from Escherichia freundii induced by hog gastric mucin. *J Biol Chem*. 1981;256:3900–3905.
31. Scott JE. Morphometry of cupromeronic blue-stained proteoglycan molecules in animal corneas, versus that of purified proteoglycans stained in vitro, implies that tertiary structures contribute to corneal ultrastructure. *J Anat*. 1992;180:155–164.
32. Saito H, Yamagata T, Suzuki S. Enzymatic methods for the determination of small quantities of isomeric chondroitin sulfates. *J Biol Chem*. 1968;243:1536–1542.
33. Yamagata T, Saito H, Habuchi O, Suzuki S. Purification and properties of bacterial chondroitinases and chondrosulfatases. *J Biol Chem*. 1968;243:1523–1535.
34. Michelacci YM. Collagens and proteoglycans of the corneal extracellular matrix. *Braz J Med Biol Res*. 2003;36:1037–1046.
35. Young RD, Tudor D, Hayes AJ, et al. Atypical composition and ultrastructure of proteoglycans in the mouse corneal stroma. *Invest Ophthalmol Vis Sci*. 2005;46:1973–1978.
36. Caterson B, Christner JE, Bake JR, Couchman JR. Production and characterization of monoclonal antibodies directed against connective tissue proteoglycans. *Fed Proc*. 1985;44:386–393.
37. Caterson B, Christner JE, Baker JR. Identification of a monoclonal antibody that specifically recognizes corneal and skeletal keratan sulfate, monoclonal antibodies to cartilage proteoglycan. *J Biol Chem*. 1983;258:8848–8854.
38. Mehmet H, Scudder P, Tang PW, Hounsell EF, Caterson B, Feizi T. The antigenic determinants recognized by three monoclonal antibodies to keratan sulphate involve sulphated hepta- or larger oligosaccharides of the poly(N-acetyllactosamine) series. *Eur J Biochem*. 1986;157:385–391.
39. Takagi M, Ono Y, Maeno M, Miyashita K, Omiya K. Immunohistochemical and biochemical characterization of sulphated proteoglycans in embryonic chick bone. *J Oral Sci*. 1997;39:156–163.
40. Couchman JR, Caterson B, Christner JE, Baker JR. Mapping by monoclonal antibody detection of glycosaminoglycans in connective tissues. *Nature*. 1984;307:650–652.
41. Ehlers N, Bramsen T. Central thickness in corneal disorders. *Acta Ophthalmol*. 1978;56:412–416.
42. Hedbys BO, Mishima S. The thickness-hydration relationship of the cornea. *Exp Eye Res*. 1966;5:221–228.
43. Bettelheim FA, Plessy B. The hydration of proteoglycans of bovine cornea. *Biochim Biophys Acta*. 1975;381:203–214.
44. Palka BP, Sotozono C, Tanioka H, et al. Structural collagen alterations in macular corneal dystrophy occur mainly in the posterior stroma. *Curr Eye Res*. 2010;35:580–586.
45. Funderburgh JL, Caterson B, Conrad GW. Distribution of proteoglycans antigenically related to corneal keratan sulfate proteoglycan. *J Biol Chem*. 1987;262:11634–11640.

Investigative Ophthalmology & Visual Science

46. Scott JE, Haigh M. Keratan sulphate and the ultrastructure of cornea and cartilage: a 'stand-in' for chondroitin sulphate in conditions of oxygen lack. *J Anat*. 1988;158:95–108.
47. Lewis D, Davies Y, Nieduszynski IA, et al. Ultrastructural localization of sulfated and unsulfated keratan sulfate in normal and macular corneal dystrophy type I. *Glycobiology*. 2000;10:305–312.
48. Scott JE. Supramolecular organization of extracellular matrix glycosaminoglycans, in vitro and in the tissues. *FASEB J*. 1992; 6:2639–2645.
49. Plaas AH, West LA, Midura RJ. Keratan sulfate disaccharide composition determined by FACE analysis of keratanase II and endo-beta-galactosidase digestion products. *Glycobiology*. 2001;11:779–790.
50. Plaas AH, West LA, Thonar EJ, et al. Altered fine structures of corneal and skeletal keratan sulfate and chondroitin/dermatan sulfate in macular corneal dystrophy. *J Biol Chem*. 2001;276: 39788–39796.